Subnanometer Porous Thin Films by the Co-assembly of Nanotube Subunits and Block Copolymers

Ting Xu,*,†,‡,§ Nana Zhao,† Feng Ren,⊥ Rami Hourani,† Ming Tsang Lee,⊥ Jessica Y. Shu,† Samuel Mao,⊥ and Brett A. Helms∥

†Department of Materials Science and Engineering ‡Department of Chemistry, University of California, Berkeley, California, §Materials Sciences Division, Lawrence Berkeley National Laboratory ⊥Department of Mechanical Engineering, University of California, Berkeley, California, and ∥The Molecular Foundry, Lawrence Berkeley National Laboratory, Berkeley, California

ABSTRACT Porous thin films containing subnanometer channels oriented normal to the surface exhibit unique transport and separation properties and can serve as selective membranes for separation and protective coatings. While molecularly defined nanoporous inorganic and organic materials abound, generating flexible nanoporous thin films with highly aligned channels over large areas has been elusive. Here, we developed a new approach where the growth of cyclic peptide nanotubes can be directed in a structural framework set by the self-assembly of block copolymers. By conjugating polymers to cyclic peptides, the subunit of an organic nanotube can be selectively solubilized in one copolymer microdomain. The conjugated polymers also mediate the interactions between nanotube and local medium and guide the growth of nanotubes in a confined geometry. This led to subnanometer porous membranes containing high-density arrays of through channels. This new strategy takes full advantage of nanoscopic assembly of BCPs and the reversibility of organic nanotube growth and circumvents impediments associated with aligning and organizing high aspect ratio nano-objects normal to the surface. Furthermore, the hierarchical coassembly strategy described demonstrates the feasibility of synchronizing multiple self-assembly processes to achieve hierarchically structured soft materials with molecular level control.

KEYWORDS: subnanometer porous membrane · nanotube · cyclic peptide–polymer conjugate · block copolymer

There are growing demands to fabricate polymeric thin films with vertically aligned subnanometer channels for applications including carbon capture, gas separation, water desalination, batteries, fuel cell membranes, and solar-fuel conversion.[1−8] Obtaining molecular level control over the pore size, shape, and surface chemistry is a critical bottleneck and has been investigated across many disciplines. Inorganic or hybrid porous materials, such as zeolites and metal organic frameworks where pore size can be readily tailored from a few tenths to several nanometers, have achieved some success along these lines.[9,10] However, it remains a challenge to orient the channels over macroscopic distances and to process these materials on flexible substrates.

Polymers, on the other hand, are readily processed at low cost as thin films or multilayered laminates with little, if any, constraints on chemical structure and thickness of the individual layers. Hypercrosslinked polymer networks can provide pores as small as a few tenths of nanometers, but the size distribution of the pores is broad and the spatial arrangement is random which impedes selective transport.[11,12] Alternatively, by using block copolymers (BCPs), it is now routine to produce nanoporous thin films with nearly monodisperse aligned pores as small as 3 nm.[13−15] However, even the smallest pore size obtained in a BCP thin film is too large for the selective molecular transport required in advanced applications including the aforementioned areas. The dimensions of the individual polymer chains, the surface energy required to stabilize such small pores, the thermodynamics governing the microphase separation of BCPs, and the relaxation behavior of synthetic polymers pose insurmountable obstacles in reducing channel diameters to the subnanometer level using polymers alone.[16−18]

Composite films have been fabricated using preformed nanotubes such as carbon nanotubes (CNTs).[4,19] However, there are no effective means to orient preformed nanotubes normal to the surface over macroscopic distances.[20,21] Thus, vertically aligned CNT forests have been grown on substrates, yet it remains nontrivial to backfill with matrix materials between CNTs to achieve lift-off from the underlying substrate generating through channels.[4,19] CNTs prepared *via* this route are still subject to some degree of heterogeneity in their pore size distribution, which may be a further limiting factor in their implementation as selective membranes. Interior modification of preformed nanotubes to enhance selectively also represents a significant hurdle.

*Address correspondence to tingxu@berkeley.edu.

Received for review November 13, 2010 and accepted December 23, 2010.

Published online January 06, 2011
10.1021/nn103083t

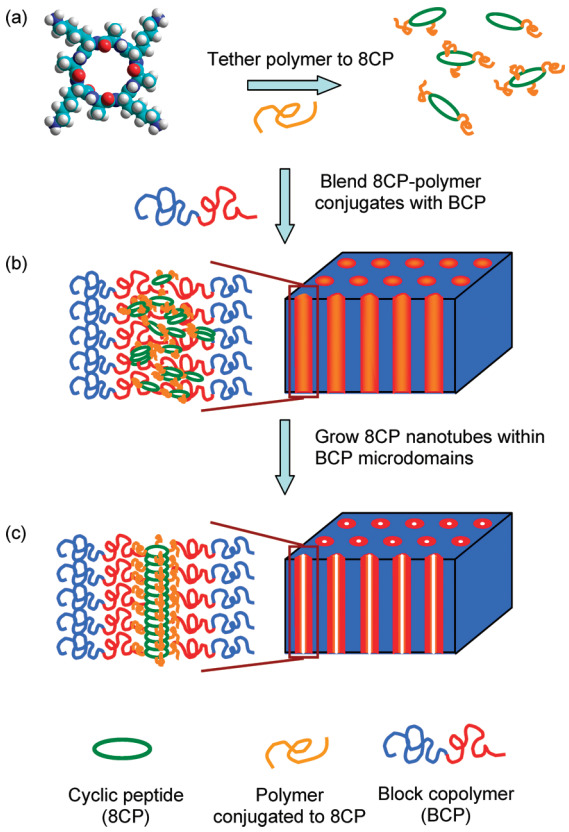

Figure 1. Schematic drawing describing the process to generate subnanometer porous films *via* directed coassembly of cyclic peptide (8CP) and a block copolymer (BCP) forming cylindrical microdomains. Polymers are first covalently linked to the side chains of 8CPs to form 8CP−polymer conjugates. The attached polymers effectively mediate the interactions between 8CPs and BCP. Upon blending with BCPs, 8CP−polymer conjugates are selectively sequestered within one BCP component and, subsequently, assemble into nanotubes spanning the entire film thickness to produce subnanometer porous films.

In contrast to CNTs, subnanometer tubular materials with precise control over the pore size, shape, and surface chemistry can be produced by assembling organic motifs such as cyclic peptides, dendrimers, DNA, surfactants, and rosettes.[3,22−27] Unlike preformed nanotubes such as CNTs, the formation of nanotubes based on organic subunits is reversible, as they are governed by specific intermolecular interactions, like hydrogen bonding or electrostatic interactions. A directed, synergistic coassembly of nanotube subunits and BCPs may allow one to direct the formation of nanotubes within the nanoscopic domains established by the BCPs so as to manipulate the spatial organization and macroscopic orientation of nanotubes. It completely eliminates the need to prepare nanotubes of uniform length, since the number of subunits comprising the nanotube can easily be varied so that the nanotube length is tailored to be equal to the film thickness, thus producing porous films with nanotubes that span the entire film.

RESULTS AND DISCUSSIONS

The generation of subnanometer porous films by coassembling cyclic peptides (CPs) and a BCP with a cylindrical morphology is schematically shown in Figure 1. CPs consist of an even number of alternating D- and L-amino acids residues assemble into hollow tubular structures (cyclic peptide nanotubes, or CPNs), propagated by hydrogen bonding between amino acid residues on adjacent rings. The CPNs are highly stable across a broad range of organic solvents, pHs, and temperatures. The internal diameter of CPNs depends on the size of the cyclic peptide ring and can be varied from a few angstroms to a few nanometers.[1,28,29] Figure 1a depicts a CP with a sequence of ([D-Ala-L-Lys]$_4$) (called 8CP) that stacks to form nanotubes (called 8CPNs), ∼0.7−0.8 nm in diameter.[22,30] Polymers are tethered to the 8CP side chains to improve solubility and modify the nanotube growth.[31−33] The tethered polymers can also be used to mediate the CP/BCP interactions to selectively sequester the 8CP−polymer conjugates into one BCP microdomain, as schematically shown in Figure 1b. The 8CPs can assemble into nanotubes within the BCP cylindrical microdomains to produce porous films with well-defined channels oriented normal to the surface, as shown in Figure 1c.

The success of the coassembly relies on a delicate balance between the thermodynamics and kinetics of two self-assembly processes, i.e. nanotube growth and BCP microphase separation, along with the interactions governing the integration of the nanotubes

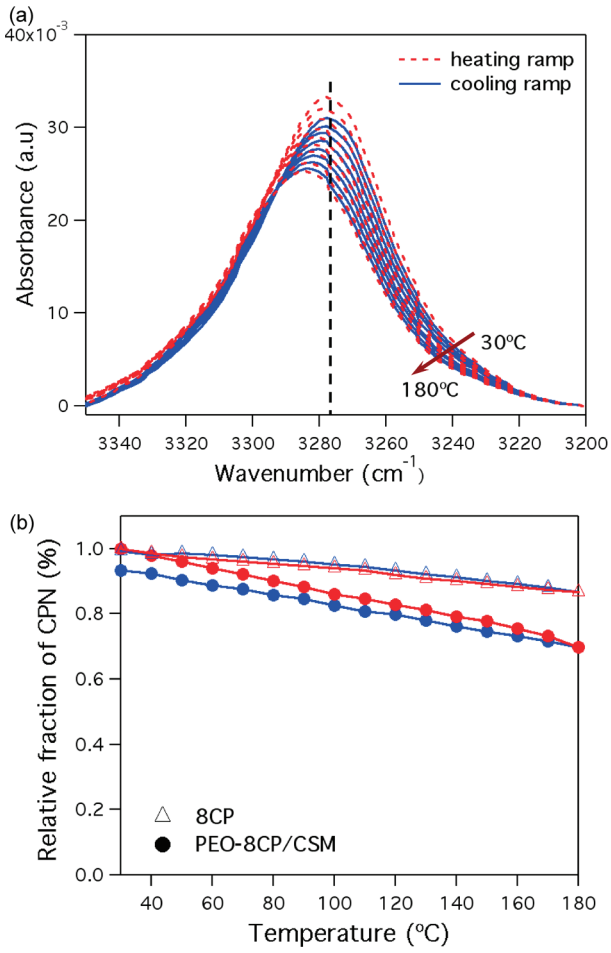

Figure 2. ***In situ*** **FTIR studies on the growth of 8CPNs under thermal treatments. (a) Amide region of the FTIR spectra of a blend of 8CP−PEO/CSM (2:10** ***wt*** **ratio) during a heating (dash line, red) and cooling cycle (solid line, blue) from 30 to 180 °C. (b) Fraction of 8CPNs based on the absorbance at 3277 cm^{-1} as a function of temperature for 8CP alone (Δ) and a blend of 8CP−PEO/CSM (●) during the heating (red) and cooling (blue) cycle. Thermoreversible nanotube growth can be clearly observed. For the measurements, the samples were cast between two NaCl plates. The heating/cooling rate is 20 °C/min, and each spectrum was collected 5 min after reaching the targeted temperature.**

within the BCP microdomain. In particular, sequestering CPs into the BCP microdomains cannot hinder the nanotube formation by the CPs. The nanotube growth must be confined by the structural framework afforded by the self-assembly of the BCP to ensure vertical alignment. Thus, the driving force to form nanotubes and the nanotube/BCP interactions that spatially restrict nanotube growth selectively within the BCP microdomain must be carefully balanced.

Two polystyrene−*block*−poly(methyl methacrylate) (PS−*b*−PMMA) BCPs were used. One has a M_w of 82 kDa (PDI = 1.07), a PMMA volume fraction of ~0.5 and forms a lamellar microdomain morphology (called LSM). The other has a M_w of 74 kDa (PDI = 1.07), a PMMA volume fraction of ~0.3, and forms a cylindrical microdomain morphology (called CSM). LSM and CSM BCPs can be solution processed into thin films on different substrates where the BCP microdomains are oriented normal to the surface.[34,35] Polymers conjugated to the CP side chains mediate the interactions between the CPs and BCPs. The number of polymers conjugated to one CP and the molecular weight of the polymer also dictate the CPN growth and, consequently, the average length of CPNs.[33] Three polymers, PS (M_w = 3 kDa), poly(ethylene oxide) (PEO) (M_w = 3.3 kDa), and PMMA (M_w = 5 kDa) were covalently linked to the 8CP side chains using two types of chemistries detailed in the Supporting Information (SI 1). The resulting PS−8CP and PEO−8CP conjugates have an average polymer:8CP ratio of 1.6. For both cases, we attempted to separate conjugates with well-defined polymer:8CP ratios but were not successful due to the strong interactions between 8CPs. We also synthesized conjugates using 8CP mutants with only one or two sites for polymer conjugation. As discussed below, the effects of the number of polymers attached are less important than the chemical nature of polymers and will be discussed in a future publication.

In toluene, 8CP−PS and 8CP−PEO conjugates form polymer-covered CPNs that are ~200 nm in length and ~2.5−3 nm in diameter. This is consistent with 8CPs forming subnanometer nanotubes, as reported

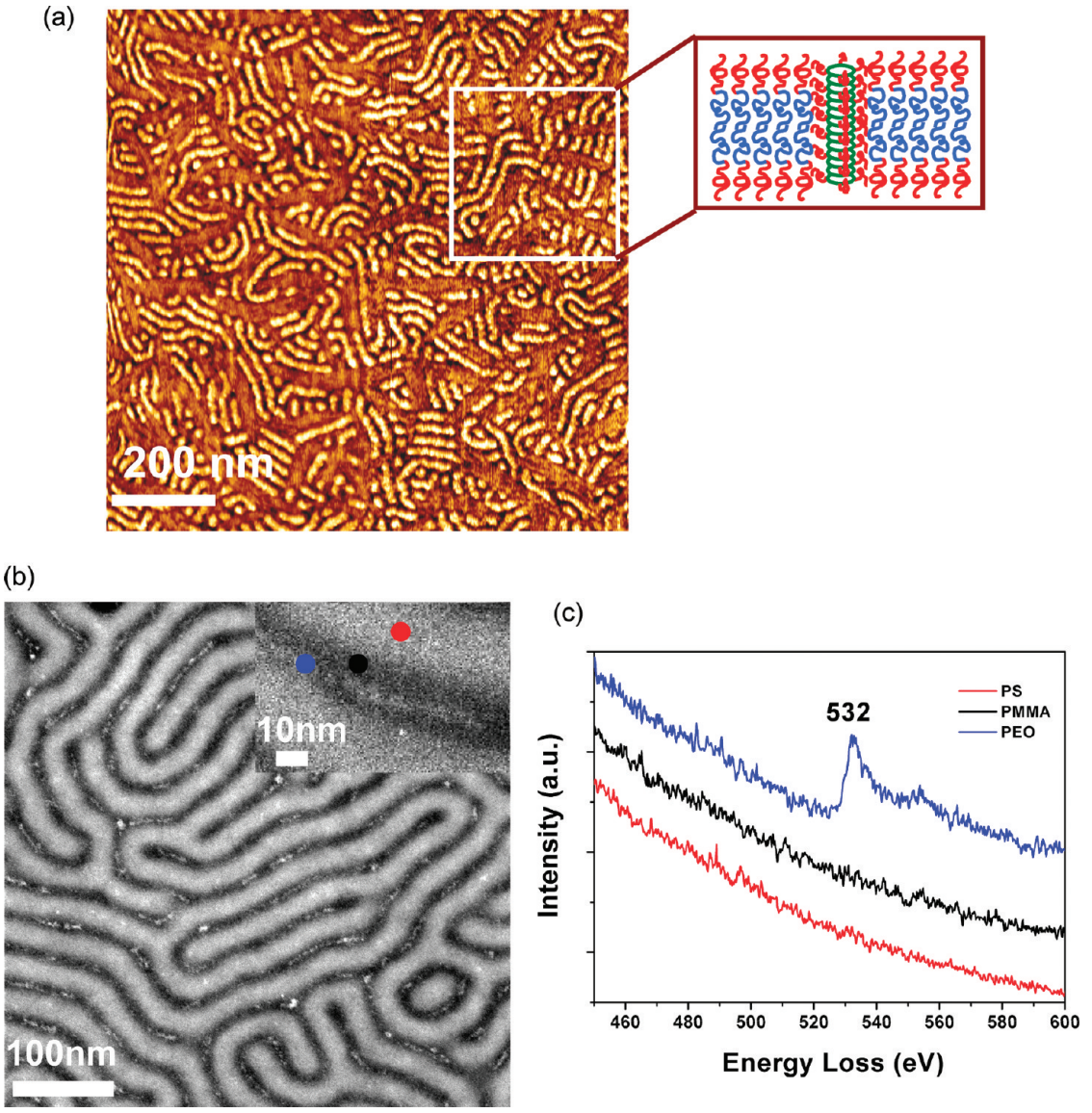

Figure 3. AFM and STEM images of blends of polymer−8CP and BCP, showing that the interactions between the conjugated polymers and each BCP block are key parameters to direct their coassembly. (a) AFM height image of ~32 nm thin films of 8CP−PS/LSM (3:10 *wt* ratio), where PS-covered CPNs phase separate from LSM. This increased the interfaces between PS and PMMA as schematically shown. Individual PS-covered CPNs laying parallel to the surface can be clearly seen. (b) HAADF-STEM image of a ~32 nm thin film of PEO−8CP/LSM (3:10 *wt* ratio), where PEO-covered CPNs are selectively sequestered in the PMMA lamellae. The bright and dark lamellae correspond to PS and PMMA microdomains, respectively. (c) EELS spectra that identify the PS, PMMA, and PEO regions, respectively.

previously.[22,30] PMMA−8CP has an average PMMA:8CP ratio of 3.3. The higher PMMA molecular weight (M_w = 5 kDa) and the PMMA:8CP ratio suppress the CPN growth and lead to a shorter average length of PMMA-covered 8CPNs in toluene, in comparison to that of PEO−8CPNs (~45 *vs* 200 nm). In any case, the nanotubes are polydisperse in length.

To circumvent difficulties associated with vertical alignment of preformed nanotubes, we will take advantage of the reversibility of nanotube formation, coassemble the subunit of nanotubes with BCPs and grow nanotubes in the nanoscopic framework defined by the BCP. 8CPN formation is governed by the interring hydrogen bonding and is thermo-reversible. Many BCPs self-assemble into ordered nanostructures upon heating and the nanostructures can be retained upon cooling. *In situ* Fourier transform infrared (FTIR) spectroscopy was used to monitor the growth of 8CPN as a function of temperature upon blending with BCPs.[22] Figure 2a shows the amide A region of the FTIR spectra of a blend of 8CP−PEO/CSM (2:10 *wt* ratio) and the absorbance at 3277 cm^{-1} reflects the CPN formation.[22] Upon heating to 180 °C, the absorption peak shifts to a higher wavenumber due to the disassembly of 8CPNs. Upon cooling, the absorption peak shifts back to 3277 cm^{-1}. The Figure 2b shows the estimated fraction of 8CPN formation based on the absorbance at 3277 cm^{-1} for 8CP alone and a blend of

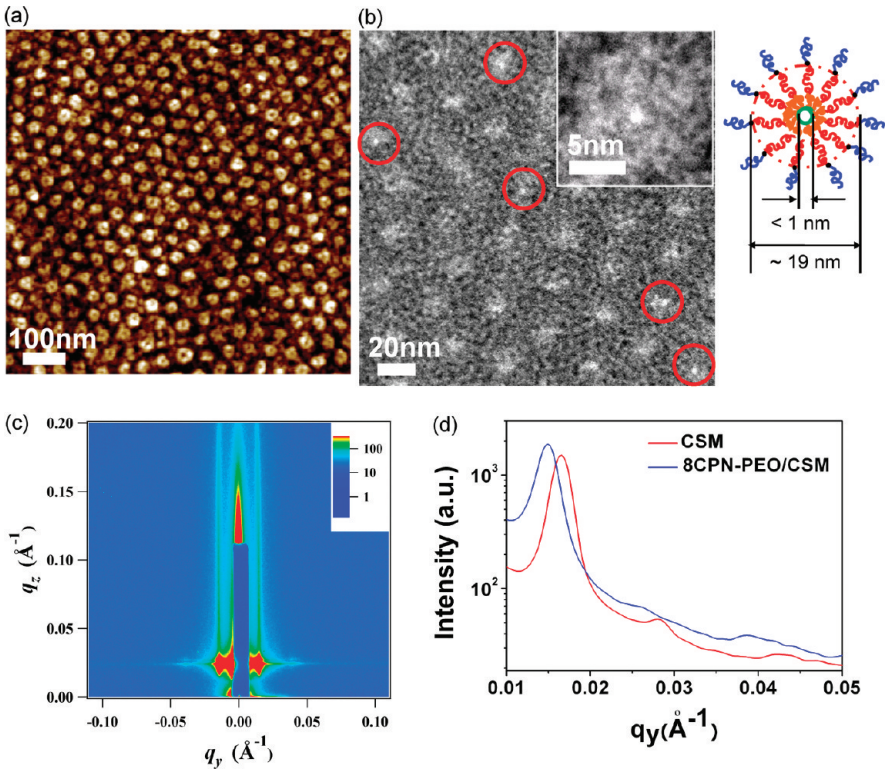

Figure 4. Structural characterization of the thin films of blends of PEO−8CP and CSM, confirming hexagonally packed 8CPNs, are oriented normal to the surface throughout the entire film thickness. (a) AFM phase image of a ~32 nm thin film of PEO−8CP/CSM (2:10 *wt* ratio). The dark core corresponds to PEO-covered 8CPNs. (b) TEM image of an in-plane view of a similar PEO−8CP/CSM (2:10 *wt* ratio) thin film. The image is taken at an under-focus of 2 μm to enhance contrast. 8CPNs spanning the film thickness can be seen in the center of PMMA domains. Red circles indicate the CPNs aligned parallel to the electron beam. Inset shows the zoomed-in image of an in-plane view of one 8CPN. TEM images taken under the same conditions as for CSM and PEO/CSM can be found in the Supporting Information. The coassembly of PEO−8CP conjugates and CSM in thin films over macroscopic distances was characterized using GISAXS. (c) GISAXS pattern of a ~32 nm thin film of PEO−8CP/CSM at an incident angle of $\alpha_c = 0.19°$. (d) q_y scans at $q_z = 0.025$ Å^{-1} for thin films of PEO−8CP/CSM and CSM. Upon incorporation of PEO−8CP, the lateral spacing increases ~3 nm from 38 to 41 nm. The combined GISAXS, AFM, and TEM results confirm incorporation of one PEO−8CPN per PMMA cylindrical microdomain at a PEO−8CP:CSM ratio of 2:10 by weight.

8CP−PEO/CSM (2:10 *wt* ratio) during a heating and cooling cycle from 30 to 180 °C. 8CPN is fairly stable at elevated temperature and the 8CPN formation process is fully reversible. Attaching polymers to 8CP destabilizes the nanotubes and upon heating to 180 °C, nearly one-third of PEO−8CPNs disassemble in the mixture of 8CP−PEO and CSM. The formation of PEO-covered 8CPNs is thermally reversible and, upon cooling to 30 °C, a large fraction (>90%) of the initial nanotubes reform. Consequently, the coassemblies shown schematically in Figure 1 may occur with the growth of nanotubes within BCP microdomains.

The coassembly of polymer−8CP conjugates and BCP was studied. Figure 3a shows an atomic force microscopy (AFM) image of a ~ 32 nm thin film of a 8CP−PS/LSM (3:10 *wt* ratio) blend after thermal annealing at 178 °C for 4−5 h and cooling to room temperature over 10−15 min. The Si substrates were modified to orient the BCP microdomains normal to the surface.[35] Upon blending with LSM, 8CP−PS conjugates retain very strong tendencies to form nanotubes, as confirmed by attenuated total reflectance (ATR)-FTIR (Supporting Information Figure S2a). PS-covered CPNs, a few hundred nanometers in length, are seen to orient parallel to the surface of the film and phase separate from the LSM.[22,28,32] Notably, a large portion of polymer-covered 8CPNs are oriented perpendicular, rather than parallel, to the LSM lamellae, forming "T" junction defects that increase the interfacial area between the polymer-covered 8CPNs and BCP blocks. Thus, the energy gained to form nanotubes is higher than the energetic penalty associated with the additional PMMA/PS interfaces. To synchronize the self-assembly processes of BCP and 8CP and confine the nanotube growth selectively within a BCP microdomain, either the tendency for the nanotube growth should be further suppressed or the interfacial interactions between the conjugated polymers and one BCP block must be increased.

Coating 8CPNs with PMMA was likewise not able to circumvent these energetic considerations toward confining the nanotube growth within BCP microdomains. The inter-ring distance between CPs is ~0.47 nm.[30] Conjugating polymer chains with a larger radius

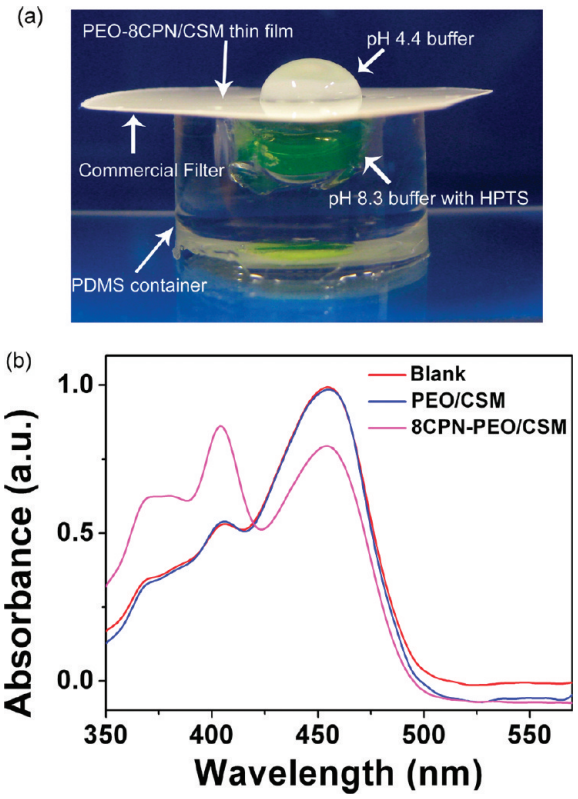

Figure 5. Proton transport measurement confirm the CPNs are macroscopically aligned normal to the film thickness and span the film. (a) Photo of the transport measurement setup. The subnanometer porous film was processed onto a commercial filter. The indicator solution (10 μM HPTS in 25 mM KH_2PO_4 with 10 mM KCl at pH 8.3) was deposited into a 150-μL PDMS container and covered with one of the fabricated thin film membranes. Subsequently, 50 μL of 25 mM KH_2PO_4 at pH 4.4 was introduced to the top of the thin film. The UV−vis spectrum of HPTS buffer solution was collected after 2 min. (b) UV−vis absorption spectra of HPTS buffer solution before and after the acidic buffer solution was deposited onto the PEO−8CPN/CSM and PEO/CSM thin films. For PEO/CSM thin films, no pH change was observed. In contrast, the decrease in pH for the HPTS buffer solution was clearly seen for PEO−8CPN/CSM thin films due to the proton transport through the CP nanotubes, which is consistent with PEO−8CPNs spanning the entire film thickness.

of gyration suppresses the nanotube growth.[33] Increasing the number of polymers conjugated to each CP also has a similar effect. 8CP−PMMA, with a higher molecular weight of PMMA (5 k *vs* 3 kDa) and average polymer:8CP ratio (3.3 *vs* 1.6), was used to blend with LSM, but was not effective in exclusively sequestering PMMA-covered CPNs within the PMMA lamellae as shown in Supporting Information, Figure S2b. Further increasing the polymer molecular weight and polymer:8CP ratio may suppress the CPN growth. However, this also disrupts the registry between 8CPs and compromises the linearity and transport properties of CPNs.

As tethered polymers strongly mediate the interactions between CPNs and each BCP block and determine the interfacial interactions associated with the defect formation, attaching a polymer with strong repulsive interactions with one BCP block, the energy penalty to form defects shown in Figure 3a would be high. This should provide a driving force to solublize polymer−8CP conjugates and confine the 8CPN growth exclusively within one BCP microdomain. The PS block has considerably stronger repulsive interactions with PEO than with PMMA.[36,37] PEO also has weak favorable interactions with PMMA.[38] Figure 3b shows a high angle annular dark field scanning TEM (HAADF-STEM) image of a ~32 nm thin film of PEO−8CP/LSM (3:10 *wt* ratio) that reflects mainly the *Z*-contrast among various components. The electron energy loss spectra (EELS) (Figure 3c) identify the different chemical constituents and indicate that PEO−8CPNs are selectively sequestered to the center of the PMMA lamellar microdomains.

Careful inspection of Figure 3b shows CPNs are randomly oriented within the PMMA lamellae. Directed growth of CPNs in a cylindrical microdomain may lead to vertical alignment of nanotubes. Figure 4a shows an AFM image of a ~32 nm thin film of PEO−8CP/CSM (2:10 *wt* ratio). Hexagonally packed core−shell cylinders oriented normal to the surface of the film are observed. The core, ~4 nm in diameter, agrees with the PEO−8CPN sequestered to the center of cylinder.[31] In toluene, PEO−8CPs form nanotubes of ~200 nm in length, much larger than the film thickness. The ATR-FTIR spectra of two films of PEO−8CP/CSM (Supporting Information SI 4) that were quenched and slowly cooled from 178 °C, respectively, show that PEO−8CPs are first incorporated within the PMMA cylindrical

microdomains and subsequently reassembled into PEO−8CPNs upon cooling. This underscores the importance of the reversibility of the assembly of CPNs that enables the length of the CPN to be adjusted to the BCP film thickness. At a lower PEO−8CP/CSM ratio, only a small fraction of cylindrical microdomains shows core−shell morphology. At the PEO−8CP/CSM ratio of 3:10, the vertical alignment of cylindrical microdomains is compromised, most likely due to the diffusion of PEG−8CP to the underlying brush layer that compromises the neutron condition of the substrate.

Figure 4b shows the in-plane TEM image of a film of a ~32 nm thin film of PEO−8CP/CSM (2:10 *wt* ratio). The image was deliberately taken under-focused to enhance contrast (Supporting Information SI 5−SI 6).[39,40] Subnanomater pores, arising from the PEO−8CPNs, are seen in the center of PMMA cylindrical microdomains, as shown in the inset. Since the aspect ratio of the CPN is over 40, it is mandatory that the PEO−8CPNs be straight, oriented normal to the film surface, and spanning the entire film for these subnanometer pores to be observable. Tilt TEM experiments further confirmed this where 1 degree tilting leads to disappearance of the CPNs for the TEM studies (Supporting Information SI 7). Figure 4c shows the grazing incidence small-angle X-ray scattering (GISAXS) pattern of the same film. The GISAXS pattern was collected at an incidence angle of 0.19° where the X-rays probe the entire film thickness and concludes that the cylindrical microdomains of PMMA/PEO−8CP orient normal to the film surface. In Figure 4d, q_y scans at q_z = 0.023 Å^{-1} show that the in-plane periodicity of the cylindrical microdomains increased ~3 nm uniformly across the film with the addition of PEO−8CPs with CSM.[41] At this incidence angle, the footprint of X-rays exceeds 1.5 cm^2. The GISAXS results reflect nanostructures averaged over these areas and confirm the uniformity of vertically aligned CPN distributed over macroscopic distances.

To further confirm that the CPNs span the entire film thickness, proton transport measurements were performed by segregating a pH 4.4 buffer solution from an aqueous solution of the pH-sensitive dye, 8-hydroxypyrene-1,3,6-trisulfonic acid trisodium salt (HPTS), with a thin film of PEO−8CPN/CSM processed on a commercial filter or, as a control, a thin film of PEO/CSM, as shown in Figure 5a.[1,3] The UV−vis spectra of the HPTS buffer solutions (Figure 5b) shows that the PEO/CSM film effectively blocks proton transport, and no change in the UV−vis spectrum was observed. For PEO−8CPN/CSM, however, a pH change was seen within 2 min. Time-dependent measurements (Supporting Information Figure S8c) also confirmed the proton transport in the 8CPN-embedded film. Transport measurements using thin film membranes can be compromised by defects in the structure upon fabrication and handling. As a quantitative measure of film integrity, gas transport measurements across the same film was examined (Supporting Information SI 9). Using the setup shown in Figure S10 (Supporting Information), transport of two types of gases, carbon dioxide and neopentane, through PEO−8CPN/CSM thin films was measured. The gas permeance was higher for the smaller gas molecule, CO_2, and confirmed the size-selective transport through subnanometer 8CPNs (Supporting Information S 11, Table S3).

In summary, we used one type of subunit, nanotube-forming cyclic peptides, and one structural framework, a BCP, as an example and demonstrated that subnanometer porous membranes can be readily fabricated over macroscopic distances by growing organic nanotubes in a confined geometry. The directed coassembly approach should be applicable to other subunits and structural frameworks. This will lead one to generate porous thin films where the size and shape of the channels can be tailored by the molecular structure of the subunits.[3,42] Equally important, the studies presented here clearly demonstrate the feasibility to synchronize multiple self-assembly processes by tailoring secondary interactions between individual components. It opens a new avenue to achieve hierarchical structures in a multicomponent system simultaneously and to overcome the bottleneck to achieve functional materials using a "bottom-up" approach.

METHOD

Synthetic procedures to prepare materials used are described in detail in the Supporting Information. GISAXS measurements were performed using X-rays of wavelength 1.240 Å or 1.685 Å at an incident angle slightly above the critical angle of the polymer film. Tapping mode AFM images were collected on the same samples using silicon cantilevers (RTESP from Veeco, Inc.) with a resonant frequency of 255 Hz. ATR-FTIR spectra were collected using a NICOLET 6700 FT-IR spectrometer. TEM experiments were carried out at an accelerating voltage of 200 KeV using a JEOL 2100F STEM/TEM equipped with a Gatan Erlangshen ES500W, an Orius SC1000 CCDs, a Gatan Tridiem energy filter system, and a Gatan 806 HAADF STEM detector. For the STEM analysis, a 0.7 nm of probe size, 40 μm of condenser aperture, and 7 cm of camera length of HAADF detector were used. For proton and gas transport measurements, detailed descriptions of setup and data analysis are given in the Supporting Information.

Acknowledgment. This work was supported by the Director, Office of Science, Office of Basic Energy Sciences, of the U.S. Department of Energy under Contract No. DE-AC02-05CH11231 (N.Z., J.S., and T.X.); by Army Research Office under Contract No. W91NF-09-1-0374 (N.Z. and T.X.); by the Molecular Foundry at Lawrence Berkeley National Laboratory (B.H.); by the Center for Gas Separations Relevant to Clean Energy Technologies, an Energy Frontier Research Center funded by the U.S. Department of Energy, Office of Science, Office of Basic Energy Sciences

under Award Number DE-SC0001015 (R.H. and T.X.). GISAXS measurements were carried out at beamline 7.3.3 at Advanced Light Source and 8-ID at Advanced Photon Source at Argonne National Laboratory. Work at the Advanced Light Source and the Molecular Foundry was supported by the Office of Science, Office of Basic Energy Sciences, of the U.S. Department of Energy under Contract No. DE-AC02-05CH11231. We thank C. Zhang for assisting synthesis of 8CP−PEO and R. Gronsky, E. L. Thomas, and B. Smit, for valuable discussions.

Supporting Information Available: Figures S1−S11, complete experimental procedures, and characterization of cyclic peptide−polymer conjugates and TEM studies. This material is available free of charge *via* the Internet at http://pubs.acs.org.

REFERENCES AND NOTES

1. Ghadiri, M. R.; Granja, J. R.; Buehler, L. K. Artificial Transmembrane Ion Channels from Self-Assembling Peptide Nanotubes. *Nature* **1994,** *369*, 301–304.
2. Jirage, K. B.; Hulteen, J. C.; Martin, C. R. Nanotubule-Based Molecular-Filtration Membranes. *Science* **1997,** *278*, 655–658.
3. Percec, V.; Dulcey, A. E.; Balagurusamy, V. S. K.; Miura, Y.; Smidrkal, J.; Peterca, M.; Nummelin, S.; Edlund, U.; Hudson, S. D. *et al.* Self-Assembly of Amphiphilic Dendritic Dipeptides into Helical Pores. *Nature* **2004,** *430*, 764–768.
4. Holt, J. K.; Park, H. G.; Wang, Y.; Stadermann, M.; Artyukhin, A. B.; Grigoropoulos, C. P.; Noy, A.; Bakajin, O. Fast Mass Transport through Sub-2-Nanometer Carbon Nanotubes. *Science* **2006,** *312*, 1034–1037.
5. Striemer, C. C.; Gaborski, T. R.; McGrath, J. L.; Fauchet, P. M. Charge- and Size-Based Separation of Macromolecules Using Ultrathin Silicon Membranes. *Nature* **2007,** *445*, 749–753.
6. Shannon, M. A.; Bohn, P. W.; Elimelech, M.; Georgiadis, J. G.; Marinas, B. J.; Mayes, A. M. Science and Technology for Water Purification in the Coming Decades. *Nature* **2008,** *452*, 301–310.
7. Kohli, P.; Harrell, C. C.; Cao, Z.; Gasparac, R.; Tan, W.; Martin, C. R. DNA-Functionalized Nanotube Membranes with Single-Base Mismatch Selectivity. *Science* **2004,** *305*, 984–986.
8. Park, M. J.; Downing, K. H.; Jackson, A.; Gomez, E. D.; Minor, A. M.; Cookson, D.; Weber, A. Z.; Balsara, N. P. Increased Water Retention in Polymer Electrolyte Membranes at Elevated Temperatures Assisted by Capillary Condensation. *Nano Lett.* **2007,** *7*, 3547–3552.
9. Wang, B.; Côté, A. P.; Furukawa, H.; O'Keeffe, M.; Yaghi, O. M. Colossal Cages in Zeolitic Imidazolate Frameworks as Selective Carbon Dioxide Reservoirs. *Nature* **2008,** *453*, 207–211.
10. Banerjee, R.; Phan, A.; Wang, B.; Knobler, C.; Furukawa, H.; O'Keeffe, M.; Yaghi, O. M. High-Throughput Synthesis of Zeolitic Imidazolate Frameworks and Application to CO_2 Capture. *Science* **2008,** *319*, 939–943.
11. Germain, J.; Hradil, J.; Frechet, J. M. J.; Svec, F. High Surface Area Nanoporous Polymers for Reversible Hydrogen Storage. *Chem. Mater.* **2006,** *18*, 4430–4435.
12. Germain, J.; Frechet, J. M. J.; Svec, F. Hypercrosslinked Polyanilines with Nanoporous Structure and High Surface Area: Potential Adsorbents for Hydrogen Storage. *J. Mater. Chem.* **2007,** *17*, 4989–4997.
13. Yang, S. Y.; Ryu, I.; Kim, H. Y.; Kim, J. K.; Jang, S. K.; Russell, T. P. Nanoporous Membranes with Ultrahigh Selectivity and Flux for the Filtration of Viruses. *Adv. Mater.* **2006,** *18*, 709–7013.
14. Jeong, U.; Ryu, D. Y.; Kim, J. K.; Kim, D. H.; Wu, X.; Russell, T. P. Precise Control of Nanopore Size in Thin Film Using Mixtures of Asymmetric Block Copolymer and Homopolymer. *Macromolecules* **2003,** *36*, 10126–10129.
15. Park, S.; Lee, D. H.; Xu, J.; Kim, B.; Hong, S. W.; Jeong, U.; Xu, T.; Russell, T. P. Macroscopic 10-Terabit−per−Square-Inch Arrays from Block Copolymers with Lateral Order. *Science* **2009,** *323*, 1030–1033.
16. Leibler, L. Theory of Microphase Separation in Block Co-Polymers. *Macromolecules* **1980,** *13*, 1602–1617.
17. Jones, R. L.; Kumar, S. K.; Ho, D. L.; Briber, R. M.; Russell, T. P. Chain Conformation In Ultrathin Polymer Films. *Nature* **1999,** *400*, 146–149.
18. Priestley, R. D.; Ellison, C. J.; Broadbelt, L. J.; Torkelson, J. M. Structural Relaxation of Polymer Glasses at Sur faces, Interfaces and in between. *Science* **2005,** *309*, 456–459.
19. Hinds, B. J.; Chopra, N.; Rantell, T.; Andrews, R.; Gavalas, V.; Bachas, L. G. Aligned Multiwalled Carbon Nanotube Membranes. *Science* **2004,** *303*, 62–65.
20. Glotzer, S. C.; Solomon, M. J. Anisotropy of Building Blocks and Their Assembly into Complex Structures. *Nat. Mater.* **2007,** *6*, 557–562.
21. Bockstaller, M. R.; Mickiewicz, R. A.; Thomas, E. L. Block Copolymer Nanocomposites: Perspectives for Tailored Functional Materials. *Adv. Mater.* **2005,** *17*, 1331–1349.
22. Ghadiri, M. R.; Granja, J. R.; Milligan, R. A.; Mcree, D. E.; Khazanovich, N. Self-Assembling Organic Nanotubes Based on a Cyclic Peptide Architecture. *Nature* **1993,** *366*, 324–327.
23. Zhou, M. J.; Kidd, T. J.; Noble, R. D.; Gin, D. L. Supported Lyotropic Liquid-Crystal Polymer Membranes: Promising Materials for Molecular-Size-Selective Aqueous Nanofiltration. *Adv. Mater.* **2005,** *17*, 1850–1853.
24. Davis, J. T.; Spada, G. P. Supramolecular Architectures Generated by Self-Assembly of Guanosine Derivatives. *Chem. Soc. Rev.* **2007,** *36*, 296–313.
25. Sakai, N.; Kamikawa, Y.; Nishii, M.; Matsuoka, T.; Kato, T.; Matile, S. Dendritic Folate Rosettes as Ion Channels in Lipid Bilayers. *J. Am. Chem. Soc.* **2006,** *128*, 2218–2219.
26. Li, H.; Eddaoudi, M.; O'Keeffe, M.; Yaghi, O. M. Design and Synthesis of an Exceptionally Stable and Highly Porous Metal-Organic Framework. *Nature* **1999,** *402*, 276–279.
27. Ghadiri, M. R. Self-Assembled Nanoscale Tubular Ensembles. *Adv. Mater.* **1995,** *7*, 675–677.
28. Kim, H. S.; Hartgerink, J. D.; Ghadiri, M. R. Oriented Self-Assembly of Cyclic Peptide Nanotubes in Lipid Membranes. *J. Am. Chem. Soc.* **1998,** *120*, 4417–4424.
29. Amorin, M.; Castedo, L.; Granja, J. R. New Cyclic Peptide Assemblies with Hydrophobic Cavities: The Structural and Thermodynamic Basis of a New Class of Peptide Nanotubes. *J. Am. Chem. Soc.* **2003,** *125*, 2844–2845.
30. Hartgerink, J. D.; Granja, J. R.; Milligan, R. A.; Ghadiri, M. R. Self-Assembling Peptide Nanotubes. *J. Am. Chem. Soc.* **1996,** *118*, 43–50.
31. Couet, J.; Samuel, J. D. J. S.; Kopyshev, A.; Santer, S.; Biesalski, M. Peptide-Polymer Hybrid Nanotubes. *Angew. Chem., Int. Ed.* **2005,** *44*, 3297–3301.
32. ten Cate, M. G. J.; Severin, N.; Borner, H. G. Self-Assembling Peptide-Polymer Conjugates Comprising (D-*alt*-L)-Cyclopeptides as Aggregator Domains. *Macromolecules* **2006,** *39*, 7831–7838.
33. Couet, J.; Biesalski, M. Polymer-Wrapped Peptide Nanotubes: Peptide-Grafted Polymer Mass Impacts Length and Diameter. *Small* **2008,** *4*, 1008–1016.
34. Thurn-Albrecht, T.; Schotter, J.; Kastle, C. A.; Emley, N.; Shibauchi, T.; Krusin-Elbaum, L.; Guarini, K.; Black, C. T.; Tuominen, M. T.; Russell, T. P. Ultrahigh-Density Nanowire Arrays Grown in Self-Assembled Diblock Copolymer Templates. *Science* **2000,** *290*, 2126–2129.
35. Ryu, D. Y.; Shin, K.; Drockenmuller, E.; Hawker, C. J.; Russell, T. P. A Generalized Approach to the Modification of Solid Surfaces. *Science* **2005,** *308*, 236–239.
36. Russell, T. P.; Hjelm, R. P.; Seeger, P. A. Temperature-Dependence of the Interaction Parameter of Polystyrene and Poly(methyl methacrylate). *Macromolecules* **1990,** *23*, 890–893.
37. Epps, T. H.; Bailey, T. S.; Waletzko, R.; Bates, F. S. Phase Behavior and Block Sequence Effects in Lithium Perchlorate-Doped Poly(isoprene-*b*-styrene-*b*-ethylene oxide) And Poly(styrene-*b*-isoprene-*b*-ethylene oxide) Triblock Copolymers. *Macromolecules* **2003,** *36*, 2873–2881.

38. Ito, H.; Russell, T. P.; Wignall, G. D. Interactions in Mixtures of Poly(ethylene oxide) and Poly(methyl methacrylate). *Macromolecules* **1987,** *20*, 2213–2220.
39. Christner, G. L.; Thomas, E. L. Visualization of Polymer Interfaces by Phase Contrast ("Defocus") Electron Microscopy. *J. Appl. Phys.* **1977,** *48*, 4063–4067.
40. Roche, E. J.; Thomas, E. L. Defocus Electron Microscopy of Multiphase Polymers: Use and Misuse. *Polymer* **1981,** *22*, 333–341.
41. Jeong, U.; Ryu, D. Y.; Kho, D. H.; Lee, D. H.; Kim, J. K.; Russell, T. P. Phase Behavior of Mixtures of Block Copolymer and Homopolymers in Thin Films and Bulk. *Macromolecules* **2003,** *36*, 3626–3634.
42. Percec, V.; Ungar, G.; Peterca, M. Chemistry: Self-Assembly in Action. *Science* **2006,** *313*, 55–56.